AFRL-AFOSR-VA-TR-2016-0317

A Novel Multiscale Design of Interfaces for Polymeric Composites and Bonded Joints using Additive Manufacturing

Pavana Prabhakar
UNIVERSITY OF TEXAS AT EL PASO
500 UNIV ST ADMIN BLDG 209
EL PASO, TX 79968-0001

09/13/2016
Final Report

Air Force Research Laboratory
AF Office Of Scientific Research (AFOSR)/RTA1

REPORT DOCUMENTATION PAGE

Form Approved
OMB No. 0704-0188

1. REPORT DATE *(DD-MM-YYYY)*	2. REPORT TYPE	3. DATES COVERED *(From - To)*
14-08-2016	Final	May 1, 2015 - August 31, 2016

4. TITLE AND SUBTITLE
A Novel Multiscale Design of Interfaces for Polymeric Composites and Bonded Joints using Additive Manufacturing

5a. CONTRACT NUMBER

5b. GRANT NUMBER
FA9550-15-1-0216

5c. PROGRAM ELEMENT NUMBER

6. AUTHOR(S)
Prabhakar, Pavana

5d. PROJECT NUMBER

5e. TASK NUMBER

5f. WORK UNIT NUMBER

7. PERFORMING ORGANIZATION NAME(S) AND ADDRESS(ES)
The University of Texas at El Paso, TX

8. PERFORMING ORGANIZATION REPORT NUMBER

9. SPONSORING/MONITORING AGENCY NAME(S) AND ADDRESS(ES)
Dr. David Stargel, AFOSR/RTA, (703) 696-6961, David.Stargel@us.af.mil
Air Force Office of Scientific Research
875 North Randolph Street
Suite 325, Room 3112
Arlington VA, 22203

10. SPONSOR/MONITOR'S ACRONYM(S)
AFOSR

11. SPONSOR/MONITOR'S REPORT NUMBER(S)

12. DISTRIBUTION/AVAILABILITY STATEMENT
Distribution A - Approved for Public Release

13. SUPPLEMENTARY NOTES
None.

14. ABSTRACT
Interfaces in polymer based carbon fiber composites are critical regions that are most susceptible to delamination under static and impact loads. Debonding or delamination is observed to be a significant failure mechanism in layered composites with significant visible damage. A computational modeling approach is being developed to obtain optimized designs for interfaces and upscale the influence of interface reinforcements for damage and failure resistant designs, which will aid in improving the overall performance of the composite. Polymer additive manufacturing techniques are being explored towards constructing these optimized microscale interface designs based on the suggestions from the computational models.

15. SUBJECT TERMS
Additive Manufacturing, Composites, Delamination, Fracture Toughness, Bonded Joints

16. SECURITY CLASSIFICATION OF:			17. LIMITATION OF ABSTRACT	18. NUMBER OF PAGES	19a. NAME OF RESPONSIBLE PERSON
a. REPORT	b. ABSTRACT	c. THIS PAGE			Pavana Prabhakar
					19b. TELEPHONE NUMBER *(Include area code)*
U	U	U	UU	35	510-220-5824

INSTRUCTIONS FOR COMPLETING SF 298

1. REPORT DATE. Full publication date, including day, month, if available. Must cite at least the year and be Year 2000 compliant, e.g. 30-06-1998; xx-06-1998; xx-xx-1998.

2. REPORT TYPE. State the type of report, such as final, technical, interim, memorandum, master's thesis, progress, quarterly, research, special, group study, etc.

3. DATE COVERED. Indicate the time during which the work was performed and the report was written, e.g., Jun 1997 - Jun 1998; 1-10 Jun 1996; May - Nov 1998; Nov 1998.

4. TITLE. Enter title and subtitle with volume number and part number, if applicable. On classified documents, enter the title classification in parentheses.

5a. CONTRACT NUMBER. Enter all contract numbers as they appear in the report, e.g. F33315-86-C-5169.

5b. GRANT NUMBER. Enter all grant numbers as they appear in the report. e.g. AFOSR-82-1234.

5c. PROGRAM ELEMENT NUMBER. Enter all program element numbers as they appear in the report, e.g. 61101A.

5e. TASK NUMBER. Enter all task numbers as they appear in the report, e.g. 05; RF0330201; T4112.

5f. WORK UNIT NUMBER. Enter all work unit numbers as they appear in the report, e.g. 001; AFAPL30480105.

6. AUTHOR(S). Enter name(s) of person(s) responsible for writing the report, performing the research, or credited with the content of the report. The form of entry is the last name, first name, middle initial, and additional qualifiers separated by commas, e.g. Smith, Richard, J, Jr.

7. PERFORMING ORGANIZATION NAME(S) AND ADDRESS(ES). Self-explanatory.

8. PERFORMING ORGANIZATION REPORT NUMBER. Enter all unique alphanumeric report numbers assigned by the performing organization, e.g. BRL-1234; AFWL-TR-85-4017-Vol-21-PT-2.

9. SPONSORING/MONITORING AGENCY NAME(S) AND ADDRESS(ES). Enter the name and address of the organization(s) financially responsible for and monitoring the work.

10. SPONSOR/MONITOR'S ACRONYM(S). Enter, if available, e.g. BRL, ARDEC, NADC.

11. SPONSOR/MONITOR'S REPORT NUMBER(S). Enter report number as assigned by the sponsoring/ monitoring agency, if available, e.g. BRL-TR-829; -215.

12. DISTRIBUTION/AVAILABILITY STATEMENT. Use agency-mandated availability statements to indicate the public availability or distribution limitations of the report. If additional limitations/ restrictions or special markings are indicated, follow agency authorization procedures, e.g. RD/FRD, PROPIN, ITAR, etc. Include copyright information.

13. SUPPLEMENTARY NOTES. Enter information not included elsewhere such as: prepared in cooperation with; translation of; report supersedes; old edition number, etc.

14. ABSTRACT. A brief (approximately 200 words) factual summary of the most significant information.

15. SUBJECT TERMS. Key words or phrases identifying major concepts in the report.

16. SECURITY CLASSIFICATION. Enter security classification in accordance with security classification regulations, e.g. U, C, S, etc. If this form contains classified information, stamp classification level on the top and bottom of this page.

17. LIMITATION OF ABSTRACT. This block must be completed to assign a distribution limitation to the abstract. Enter UU (Unclassified Unlimited) or SAR (Same as Report). An entry in this block is necessary if the abstract is to be limited.

Final Technical Report (5/1/2015 - 8/31/2016)

PROJECT TITLE
A Novel Multiscale Design of Interfaces for Polymeric Composites and Bonded Joints using Additive Manufacturing

AWARD NO.: FA9550-15-1-0216

AGENCY NAME: The Air Force Office of Scientific Research (AFOSR), Arlington, VA

PROGRAM MANAGER
Mr. James Fillerup
Tel: 1-703-588-8316, E-mail: james.fillerup@us.af.mil

PRINCIPAL INVESTIGATOR
Pavana Prabhakar, Ph.D.
Assistant Professor, Mechanical Engineering
The University of Texas at El Paso
500 West University Ave., A-114, El Paso, Texas 79968-0521
Tel: (915) 747 5863, Fax: (915) 747 5019, E-mail: pprabhakar@utep.edu

Contents

Chapter 1

Introduction

Interfaces in polymer based carbon fiber composites are critical regions that are most susceptible to delamination under static and impact loads. Mechanical response types, like compression (Fig. 1.1(a)), bending (Fig. 1.1(b)) and impact (Fig. 1.1(c)) on layered composites are affected by the interface strength and toughness, the geometry and the extent of loading. Debonding or delamination is observed to be a significant failure mechanism in layered composites with significant visible damage.

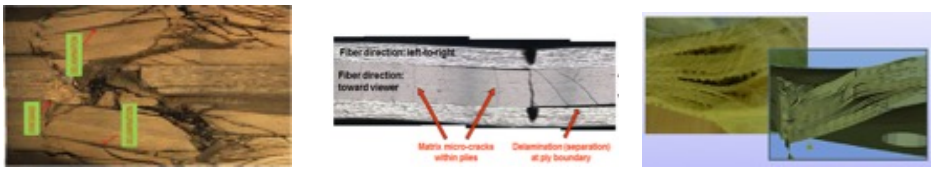

(a) (b) (c)

Figure 1.1: (a) Compressive Delamination; (b) Bending Delamination; (c) Impact Delamination

Design of interfaces is very critical for layered materials, like fiber reinforced composites and bonded joints, and smart designing techniques should be developed to minimize the damage and failure incurred by weak interfaces. Improving the strength of material is not the only route for constructing better laminated composites and bonded joints, instead, the interfaces can be engineered for specific types of loads acting and the geometry of the components. Trial and error experimental approach with changing component geometry and load combinations will be very expensive. Therefore, a robust computational model to drastically reduce the trial and error experiments for interface design has to be developed. Interface strength and toughness can be improved significantly by structural micro-reinforcements using polymer additive manufacturing. A computational modeling approach is being developed to obtain optimized designs for interfaces and upscale the influence of interface reinforcements for damage and failure resistant designs, which will aid in improving the overall performance of the composite. The strength of the composite will be increased with negligible increase in the weight and cost associated. Further, polymer additive manufacturing techniques will be tailored towards constructing these optimized microscale interface designs considering the suggestions obtained from the computational models.

1.1 Research Objectives

The overall research objective of this project are as follows:

1. Develop computational framework for designing optimum interfaces for layered composites to minimize damage and failure when subjected to static and dynamic mechanical loads as well as extreme thermal loads.

2. Develop a novel upscaling methodology to account for the influence of interface stiffeners on the macroscale failure behavior of the composite.

3. Investigate the feasibility of using additive manufacturing for constructing micro scale interfaces on composite prepregs. This will include the construction of interfaces with spatial variation to reduce effects like, edge effects on the interface delamination mechanism and damage due to high intensity impact.

4. Develop smart designs for bonded joints in aircrafts using the above developed computational design methodologies.

1.2 Background

Extensive work has been conducted by researchers that have demonstrated the influence of interfaces on the strength of the composite. Due to the presence of fiber and matrix in a fiber reinforced composites, different failure mechanisms characteristic of the constituents are observed when subjected to different types of load profiles. For example, common failure mechanisms observed when a laminate is subjected to compressive loading are kink band formation in the lamina that are aligned with the loading direction, matrix micro-cracking and delamination between laminae. Kink band formation, also known as micro-buckling, is an instability caused by the axial loading on the fibers in a lamina. In addition, a mismatch in the properties of adjacent layers causes stress concentration between laminae, resulting in the interface matrix rich region to damage and create new surfaces by releasing energy. This type of failure is referred to as delamination failure. A combination of both kinking and delamination is observed at failure. Lee and Waas[1], Lee et al. [2], Vogler et al. [3]and Pimenta et al.[4]and[5], have shown that micro-buckling in the fibers occur along with splitting when multi-directional laminates are subjected to compressive loading. Lee and Waas [1]studied the effect of fiber volume fraction on the compressive failure mode, while Yerramalli and Waas [6]studied the effect of fiber type and load multi-axiality on failure. In both of these studies, energy released by splitting (debonding) failure in combination with kinking was identified as contributing to the failure mechanism. The influence of interface delamination on the compressive strength in multidirectional fiber reinforced laminates was demonstrated through validated computational modeling by the PI (Prabhakar and Waas [7]), where the mode-II shear strength of the interface appears to influence the compressive strength of the laminate. Also, the free edge effects contributed significantly to the delamination response of the composite.

1.3 Research Plan

The proposed work deals with developing high fidelity computational approach for determining critical interfaces and smart design of the same for polymer matrix composites and bonded joints. Also, a pioneering idea towards the building the designs using additive manufacturing is investigated. The steps mentioned below were proposed:

- Task 1: Develop interactive computational framework for designing structural interfaces for layered composites: Reduced-order Critical Interface Analysis (RoCIA) and Microscale Optimized Design of Interface Truss Structures (MODITS)
- Task 2: Develop a multiscale modeling approach to upscale from microscale to macroscale
- Task 3: Investigate the feasibility of constructing structural interfaces using additive manufacturing: Fused Deposition Modeling (FDM) type of printing on Prepregs
- Task 4: Engineering the interfaces using the above formulations for aircraft bonded joints

This is a final technical report for the project with start date of May 1st, 2015 to August 31st, 2016. During this period, the project has mainly focused on Tasks 1 and 4. Chapters 2 and 3 describe the work conducted and corresponding findings within these tasks.

1.3.1 Task 1: Develop interactive computational framework for designing structural interfaces for layered composites

Under this task, a computational approach for the microscale structural designs for enhanced interfaces between layered fiber reinforced composites is being developed. The first step towards that will be formulating a reduced order finite element analysis (FEA) approach to determine critical interfaces within the composite when subjected to different types of loads. Using the stress-strain information at the interfaces determined this step, the optimized microscale structural designs for the interfaces will be determined using a combination of FEA and genetic algorithm (GA) approaches.

A novel modeling approach, called reduced-order critical interface analysis (RoCIA), is being developed to determine the critical interface within layered composites to minimize the computational cost associated with large models. The framework will also include the effects of spatial and temporal variation of the interface properties to determine the optimum interfaces.

1.3.2 Task 4: Engineering the interfaces using the above formulations for aircraft bonded joints

The goal is this task is to first investigate the feasibility of incorporating designs at the bonded regions to improve their bond strength using Fused Deposition Modeling (FDM), which is an

additive manufacturing technique for polymers. Single lap shear tests have been investigated to explore the influence of structural interfaces at the bond regions of single lap joints. The result thus far have been promising with the apparent shear strength increasing quadruple times. The design incorporated at the bond regions on the adherents have been analyzed using computational models to study their effects on the stress distribution.

1.4 Milestones Achieved: 5/1/2015-8/31/2016

The milestones achieved so far within this project are as follows:

- Chapter 2: Reduced-order Critical Interface Analysis (RoCIA) to identify critical interlaminar regions in multidirectional laminates subjected to combined tensile-temperature loading has been developed and validated.
- Chapter 3: The feasibility of constructing structural interfaces using additive manufacturing: Fused Deposition Modeling (FDM) on laminates to improve their apparent shear strength has been successfully demonstrated through single lap shear tests on bonded joints

1.5 Publications

Journal

- M. S. Islam, P. Prabhakar, "Modeling Framework for Free Edge Effects in Laminates under Thermo-Mechanical Loading". (Under Review)
- M. S. Islam, P. Prabhakar, "Interface Strengthening of Multidirectional Laminates using Additive Manufacturing". (Under Review)
- R. Garcia, E. Acuna and P. Prabhakar, "Additive Manufacturing for Improving the Strength of Adhesively Bonded Single Lap Joints for Composites". (In Prep.)

Conference

- Md S. Islam and P. Prabhakar, "Interlaminar Strengthening of Multidirectional Laminates Using Additive Manufacturing", *Additive Manufacturing of Composites and Complex - Materials, Materials Science & Technology Conference (MS&T16)*, Salt Lake Cuty, UT, Oct. 23-27, 2016. (Accepted for presentation)
- Md S. Islam and P. Prabhakar, "Free Edge Effect in Multi-directional Laminate Under Multiaxial Loading", *American Society for Composites 31st Technical Conference and ASTM Committee D30 Meeting*, Williamsburg, Virginia, September 19-22, 2016. (Accepted for presentation)

- R. Garcia, E. Acuna and P. Prabhakar, "Additive Manufacturing For Bonded Composite Joints", *American Society for Composites 31st Technical Conference and ASTM Committee D30 Meeting*, Williamsburg, Virginia, September 19-22, 2016. (Accepted for presentation)

Chapter 2

RoCIA: Novel Model for Free Edge Effects in Laminates under Thermo-Mechanical Loading

2.1 Introduction

Interlaminar regions in polymer based layered carbon fiber composites are the critical regions that are most susceptible to delamination under static and dynamic loading. Mechanical response to load types like edge-wise and through-thickness compression, bending, and dynamic impact on layered composites is influenced by interlaminar strength and toughness, the geometry and the extent of loading. Debonding or delamination is observed to be a significant failure mechanism in layered composites with considerable visible damage. Significant localized interlaminar stresses occur at the free edges of laminated composite materials due to mismatch in property between plies, which is referred to as the "free edge effect" [8]. Accurate determination of stress distribution near the free edges is very important due to their significant impact on delamination or transverse cracking. Stress state near the free edge is three dimensional in nature and classical lamination theory (CLT) is unable to determine these stresses accurately [8, 9]. Therefore, various analytical and numerical approaches such as finite difference, finite element, closed form analytical approach, boundary layer theories and layer-wise theories have been used to calculate the interlaminar stresses near the free edges.

Puppo and Evensen [10] proposed the first analytical method to determine the interlaminar stresses in a composite laminate. Pagano [11] developed a higher order plate theory to evaluate the interlaminar stresses. Few other analytical methods are: Perturbation method by Hsu and Herakovich [12]; Boundary layer theory by Tang [13], Davet and Destuynder [14], and Lin and Ko [15]; An approximate elasticity solution by Pipes and Pagano [16]; Variational principle by Pagano [17], Lekhnitskii and Fern [18]; Stress potential method by Wang and Choi [19, 20, 21, 22], Kassapoglou and Lagace [23, 24] and Webber and Morton [25]. Becker [26] used a particular warp deformation mode to investigate the free edge effects in laminates. Kassapoglou [27] generalized the principle of minimum complementary energy and force balanced method to analyze laminates

under in-plane and out-of-plane loading. Yin [28, 29] used a variational method using Lekhnitskiis stress function for laminates under combinations of mechanical loading. Later, Yin [30] used the principle of complementary energy based on polynomial stress functions to evaluate the interlaminar stresses in laminates subjected non-uniform thermal loading.

Pipes and Pagano [31] developed the first numerical method to solve the two dimensional governing elasticity equations, where finite difference method was used to calculate the interlaminar stresses of long symmetric laminate under uniform axial strain. Later, Atlus et al. [32], Bhaskar et al. [33] and Salamon [34] used three dimensional finite difference method to determine the interlaminar stresses in angle-ply laminate. Wang and Crossman [35, 36] studied symmetric composite laminate subjected to uniform axial strain and thermal loading using finite element method. Herakovich et al. [37], Isakson and Levy [38], Rybicky [39], Kim and Hong [40], Icardi and Bertetto [41], Lessard et al. [42] and Yi and Hilton [43] also used finite element method to study free edge effects in laminates. Spilker and Chou [44] used hybrid stress finite element method, Lee and Chen [45] used layer reduction technique, Robbins and Redy [46] used displacement based variable kinematic global local finite element method, Gaudenzi et al. [47] used three dimensional multilayer higher order finite element method to study similar problems.

From previous studies mentioned above, it is well established that free edge effects are dominant in multidirectional laminates and lead to very high interlaminar stresses that prematurely initiate inter-layer delamination. Therefore, determining interfaces with very large interlaminar stresses is critical for the assessment of delamination driven failure. By doing so, the interfaces most susceptible to delamination can be determined and strengthened accordingly during manufacturing to reduce their susceptibility to failure. Towards that, a Quasi-2D formulation within the finite element method (FEM) framework is established in this paper to determine delamination prone interlaminar regions in multidirectional laminates subjected to thermo-mechanical loading.

In the current paper, the variational formulation presented by Martin et al. [48] is extended for combined thermal and axial loading, referred to as "Quasi-2D" (Q-2D) formulation. The Q-2D formulation is implemented within the FEM framework to accurately determine the stress distribution near the free edges for cross-ply $([0/90]_s)$ and quasi-isotropic $([45/-45/90/0]_s)$ laminates. Comparison of the current results with previously published results and corresponding 3D model results establishes the validity and accuracy of the Q-2D model. This paper is divided into the following sections: Section 2.2 describes the mathematical formulation for the Q-2D followed by the details of the implementation within the finite element framework in Section 2.3. Discussion of results from several case studies are presented in Section 2.4 followed by conclusions.

2.2 Mathematical Formulation

Consider a laminate of length $2L$, width $2b$ and lamina/layer thickness of h as shown in Fig. 2.1(a). Tensile load is applied on the edges at $\sum_{+L}$ and $\sum_{-L}$ along the x_1 direction, and the edges at $\sum_0$ and $\sum_{2b}$ are the free edges. Further, a temperature change of ΔT occurs uniformly within the laminate. Cross-section of the laminate consisting of N layers is shown in Fig. 2.1(b).

The stress components are assumed to be independent of x_1 in regions sufficiently far from the

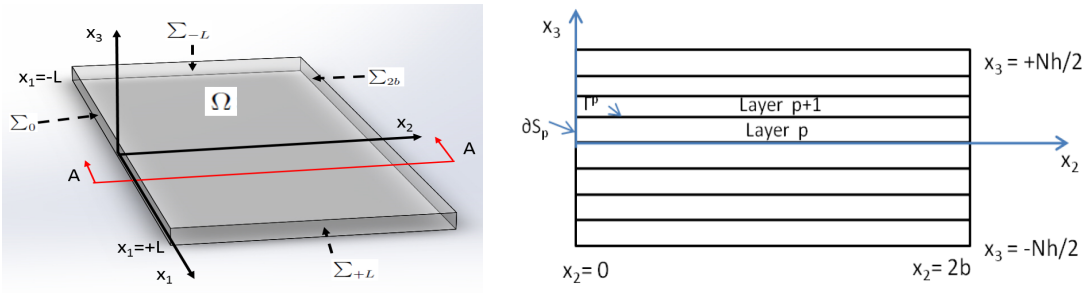

(a) (b)

Figure 2.1: (a)3D Laminate; (b) Cross-section of a 3D laminate

loading surface [31, 48], such that the displacement field $\{U\}$ can be defined as,

$$\begin{aligned} U_1(x_1, x_2, x_3) &= \tilde{U}_1(x_2, x_3) + \epsilon_{11} x_1 \\ U_2(x_1, x_2, x_3) &= \tilde{U}_2(x_2, x_3) \\ U_3(x_1, x_2, x_3) &= \tilde{U}_3(x_2, x_3) \end{aligned} \tag{2.1}$$

Here, ϵ_{11} is the uniform strain applied to the laminate along the x_1 direction. The displacement field $\{U\}$ and corresponding stress field $\{\sigma\}$ adhere to the following equations:

$$\frac{\partial \sigma_{ij}}{\partial x_j} = 0, \sigma_{ij} = a_{ijkh}\epsilon^m_{kh}, \forall i = 1, 2, 3 \text{ within } \Omega, \tag{2.2}$$

$$\epsilon_{ij}(U) = \frac{1}{2}\left(\frac{\partial U_i}{\partial x_j} + \frac{\partial U_j}{\partial x_i}\right) \text{ within } \Omega; \tag{2.3}$$

$$[U_i] = 0, [\sigma_{ij} n_j] = 0 \text{ on the interfaces } \Gamma^p; [\sigma_{ij} n_j] = 0 \text{ on } \sum_{2b} \text{ and } \sum_{0} \tag{2.4}$$

$$[\sigma_{ij} n_j] = F_i \text{ on } \sum_{+L} \text{ and } \sum_{N\frac{h}{2}}; [\sigma_{ij} n_j] = -F_i \text{ on } \sum_{-L} \text{ and } \sum_{-N\frac{h}{2}} \tag{2.5}$$

Defined by equation (2.1), introducing a trial field V with $\epsilon_{11} = 0$ and averaging equation (2.2) gives,

$$\int_\Omega \frac{\partial \sigma_{ij}}{\partial x_j} V_i d\Omega = 0, \forall V_i \text{ with i=1, 2, 3.} \tag{2.6}$$

Applying divergence theorem to the above equation yields,

$$\int_\Omega \sigma_{ij} \frac{\partial V_i}{\partial x_j} d\Omega = \int_{\sum_{+L}} F_i V_i dS - \int_{\sum_{-L}} F_i V_i dS \tag{2.7}$$

Since, V_i does not depend on x_1:

$$\int_\Omega \sigma_{il} \frac{\partial V_i}{\partial x_l} d\Omega = 0, \forall V_i \text{ with } l = 2, 3. \tag{2.8}$$

Using $\sigma_{ij} = a_{ijkh}\epsilon^m_{kh}$ yields,

$$\int_\Omega a_{ilkh}(\frac{\partial U_k}{\partial x_h} - \alpha_{kh}\Delta T)\frac{\partial V_i}{\partial x_l}d\Omega = 0, \forall V_i \text{ for i, k, h=1, 2, 3; l=2, 3} \tag{2.9}$$

where, $\{\epsilon^m\} = \{\epsilon\} - \{\alpha\}\Delta T$.

Substituting the displacement field assumption given in equation (2.1),

$$\int_\Omega a_{ilkh}(\frac{\partial \tilde{U}_k}{\partial x_h} - \alpha_{kh}\Delta T)\frac{\partial V_i}{\partial x_l}dx_1dx_2dx_3 + \epsilon_{11}\int_\Omega a_{il11}\frac{\partial V_i}{\partial x_l}dx_1dx_2dx_3 = 0 \tag{2.10}$$

Dividing the volume integral into two integrals, one along the x_1 direction, and the other in the plane of the cross section (x_2, x_3) gives,

$$\begin{aligned}\int_{-L}^{+L} dx_1 \int_S a_{ilk\beta}(\frac{\partial \tilde{U}_k}{\partial x_\beta} - \alpha_{k\beta}\Delta T)\frac{\partial V_i}{\partial x_l}dx_2dx_3 - \\ \int_{-L}^{+L} dx_1 \int_S a_{ilk1}\alpha_{k1}\Delta T\frac{\partial V_i}{\partial x_l}dx_2dx_3 + \epsilon_{11}\int_{-L}^{+L} dx_1 \int_S a_{il11}\frac{\partial V_i}{\partial x_l}dx_2dx_3 = 0,\end{aligned} \tag{2.11}$$

with $l, \beta = 2, 3$.

$$\int_S a_{ilk\beta}(\frac{\partial \tilde{U}_k}{\partial x_\beta} - \alpha_{k\beta}\Delta T)\frac{\partial V_i}{\partial x_l}dx_2dx_3 = \Delta T\int_S a_{ilk1}\alpha_{k1}\frac{\partial V_i}{\partial x_l}dx_2dx_3 - \epsilon_{11}\int_S a_{il11}\frac{\partial V_i}{\partial x_l}dx_2dx_3 \tag{2.12}$$

Applying divergence theorem on the right hand side

$$\int_{S^p} a_{ilk\beta}(\frac{\partial \tilde{U}_k}{\partial x_\beta} - \alpha_{k\beta}\Delta T)\frac{\partial V_i}{\partial x_l}dx_2dx_3 = \Delta T\int_{\partial S} a_{ilk1}\alpha_{k1}V_in_lds - \epsilon_{11}\int_{\partial S} a_{il11}V_in_lds \tag{2.13}$$

where, "s" represents a coordinate that denotes the boundary ∂S, starting at the origin of the $x_2 - x_3$ axes for the region S and traversing in counter clockwise direction. Therefore, "s" is either "x_2" or "x_3" depending on the edge on the boundary being traversed.

The above equation is modified to account for layers with different orientation in a multidirectional laminate as given below,

$$\sum_{p=1}^N \int_{S^p} a^p_{ilk\beta}(\frac{\partial \tilde{U}^p_k}{\partial x_\beta} - \alpha^p_{k\beta}\Delta T)\frac{\partial V^p_i}{\partial x_l}dx_2dx_3 = \Delta T\sum_{p=1}^N \int_{\partial S^p} a^p_{ilk1}\alpha^p_{k1}V^p_in^p_lds - \epsilon_{11}\sum_{p=1}^N \int_{\partial S^p} a^p_{il11}V^p_in^p_lds \tag{2.14}$$

Developing the right hand side of 2.14, contribution of each edge

$$\begin{aligned}\Delta T\sum_{p=1}^N \Big(\int_{-Nh/2+(p-1)h}^{Nh/2+ph} a^p_{i2k1}\alpha^p_{k1}V^p_i(2b, x_3)dx_3 - \int_{-Nh/2+(p-1)h}^{Nh/2+ph} a^p_{i2k1}\alpha^p_{k1}V^p_i(0, x_3)dx_3 \Big) \\ -\epsilon_{11}\sum_{p=1}^N \Big(\int_{-Nh/2+(p-1)h}^{Nh/2+ph} a^p_{i211}V^p_i(2b, x_3)dx_3 - \int_{-Nh/2+(p-1)h}^{Nh/2+ph} a^p_{i211}V^p_i(0, x_3)dx_3 \Big)\end{aligned} \tag{2.15}$$

Contribution of each interface,

$$\begin{aligned}\Delta T \sum_{p=1}^{N-1} \Bigg(- \int_0^{2b} (a_{i3k1}^{p+1}\alpha_{k1}^{p+1} - a_{i3k1}^{p}\alpha_{k1}^{p}) V_i^p(x_2, N\frac{h}{2} + ph) dx_2 \Bigg) \\ -\epsilon_{11} \sum_{p=1}^{N-1} \Bigg(- \int_0^{2b} (a_{i311}^{p+1} - a_{i311}^{p}) V_i^p(x_2, N\frac{h}{2} + ph) dx_2 \Bigg)\end{aligned} \tag{2.16}$$

and contribution of top and bottom

$$\begin{aligned}\Delta T \Bigg(- \int_0^{2b} a_{i3k1}^{1}\alpha_{k1}^{1} V_i^1(x_2, -N\frac{h}{2}) dx_2 + \int_0^{2b} a_{i3k1}^{N}\alpha_{k1}^{N} V_i^N(x_2, N\frac{h}{2}) dx_2 \Bigg) \\ -\epsilon_{11} \Bigg(- \int_0^{2b} a_{i311}^{1} V_i^1(x_2, -N\frac{h}{2}) dx_2 + \int_0^{2b} a_{i311}^{N} V_i^N(x_2, N\frac{h}{2}) dx_2 \Bigg)\end{aligned} \tag{2.17}$$

Equation 2.14 is a generalized 2D formulation which has the displacement field along the x_1, x_2 and x_3 directions. The input to the above formulation is the fourth order elasticity tensor of each layer of the laminate for a linear elastic material, coefficient of thermal expansions, applied external strain and change in temperature. The effective loads calculated for a laminate are applied to the 2D generalized representation of the laminate in the finite element method model explained in the following section.

2.3 Implementation of the Quasi-2D Formulation

The above formulation can be implemented in several ways within finite element method. The method developed in this paper is to modify a thin slice of a 3D model to behave like a generalized 2D model. A 3D model with a small thickness (1 mm in this case) in the x_1-direction is considered as shown in Fig. 2.2. Multi-point constraints are applied between the front and back face of the model such that the displacement fields are independent of x_1-direction. In Fig. 2.2(a), m is a nodal point on the front surface and n is the corresponding nodal point on the back surface. These two points (m and n) are tied together such that the displacements u,v and w are identical for the pair nodes. Similarly, all the nodal points on the front surface are tied with their corresponding points on the back surface, which satisfies the requirement of displacement fields being independent of the x_1-direction. This simulates the left hand side of equation (2.14). The external loads established by the right hand side of equation (2.14) are applied to the model on the edges in the $x_2 - x_3$ plane and the interfaces between the layers.

Eight noded linear hexahedral elements (C3D8 in ABAQUS notation) are used to mesh the Q-2D model as shown in Fig. 2.3(a). Very fine mesh is used near the interfaces and free edge to sufficiently capture the stress singularities within these regions. However, only one element is used along the x_1 direction to enforce multi-point constraint described above. Due to significantly large number of nodes on the front and back faces, enforcing multi-point constraints manually is cumbersome.

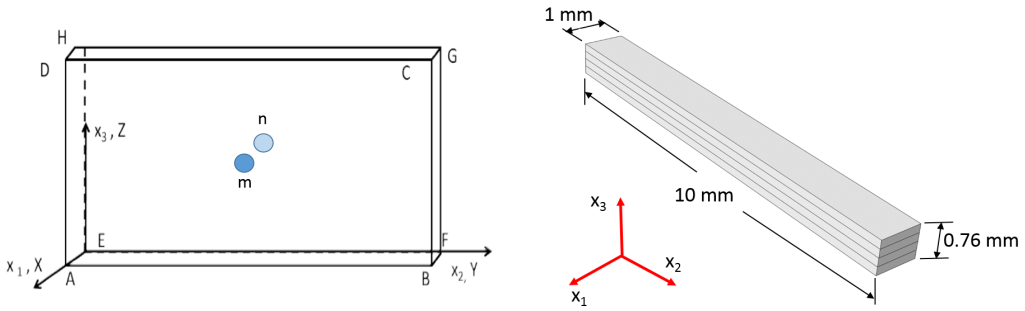

(a) (b)

Figure 2.2: 3D slice of a laminate

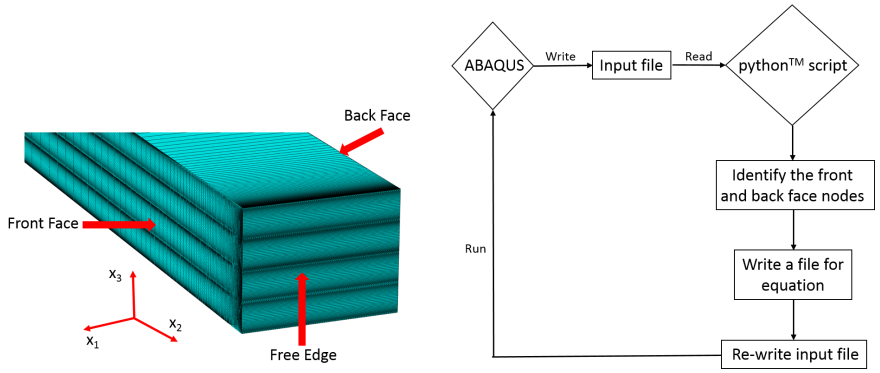

(a) (b)

Figure 2.3: (a) Typical mesh in the Q-2D model; (b) Working principle of python™ script

A python™ script is written that reads the ABAQUS input file and writes the multi-point constraints. Working procedure of the python™ script is shown in Fig. 2.3(b). The input file obtained from ABAQUS without constraints is read by the python™ script, which identifies the corresponding nodes from the front and back faces. The script then writes the constraint equations for every node in a different file and finally it rewrites the main input file, which is capable of accessing the equation file generated. Fig. 2.4(a) shows a snapshot of the re-written input file which includes the equation file as an "input" and Fig. 2.4(b) shows a snapshot of the equation file where the equation constraints are written.

As an example, Fig. 2.5 shows the boundary conditions for $[45/-45/90/0]_s$ laminate subjected to an uniform axial strain, which is derived from Equation 2.14. As mentioned in the previous section, the input to the Q-2D model is the 4th order elasticity tensor of the individual layer and the applied strain. The effective loads that depend on the elastic constants are applied as pressure along the normal directions and surface traction in the parallel directions as shown in Fig. 2.5. $\overrightarrow{x_1}$, $\overrightarrow{x_2}$ and $\overrightarrow{x_3}$ indicate the directions of load being applied, and are represented by the arrows showing the directions of load acting on different layers. The loads corresponding to $\overrightarrow{x_3}$ direction are not shown in the figure since the associated elastic constants are equal to zero in the current example. Accordingly, the effective interface loads are applied along the interfaces between the layers.

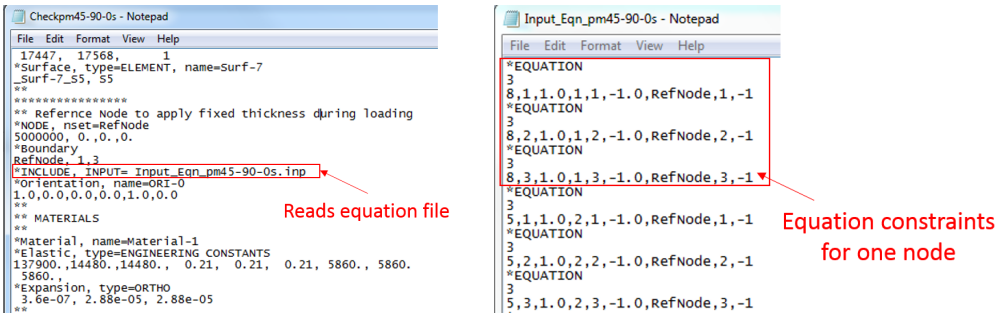

(a) (b)

Figure 2.4: Snapshot of (a) input file and (b) equation file

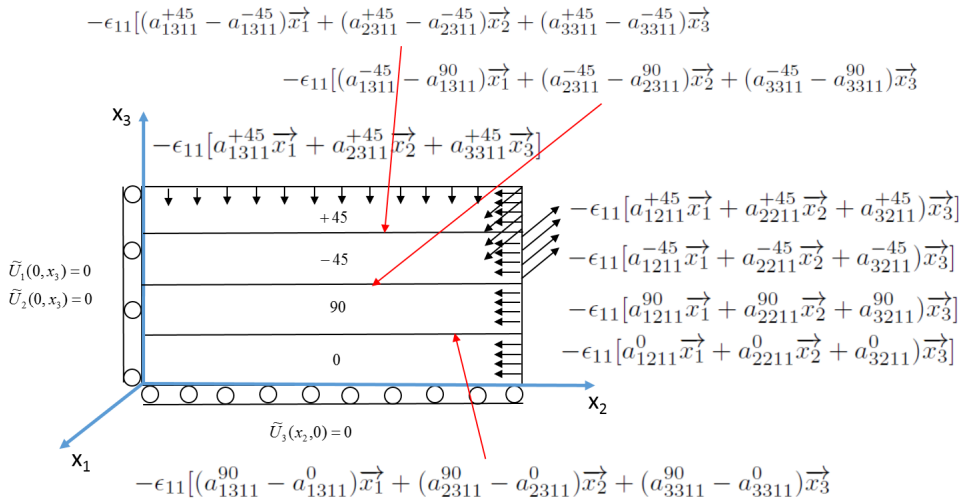

Figure 2.5: Boundary conditions for uniaxial extension

2.4 Results and Discussions

The Q-2D model is applied to several laminates subjected to three main types of loading: uniform axial extension (Section 2.4.1), uniform thermal loading (Section 2.4.2) and combined axial and thermal loading (Section 2.4.3). The results are compared with published (where available) and 3D model results to establish the reliability of the current modeling approach.

2.4.1 Case 1: Axial Loading

In this section, $[0/90]_s$ and $[45/-45/90/0]_s$ laminate subjected to an uniform axial (x-direction) strain is considered. The following material properties were used: $E_{11} = 137.9$ GPa, $E_{22} = E_{33} = 14.48$ GPa, $G_{12} = G_{13} = G_{23} = 5.86$ GPa and $\nu_{12} = \nu_{13} = \nu_{23} = 0.21$, which correspond to a high modulus graphite/epoxy laminate [49]. The $[0/90]_s$ cross-ply laminate subjected to an uniform axial (x_1-direction) strain has been previously investigated by Zhang et al. [8], Tahani and Nosier [9], Wang and Crossman [36], Nguyen and Caron [49], Carreira et al. [50] and Zhen et al.

[51]. Fig. 2.6 shows the comparison interlaminar stress distribution at the 0/90 interface of $[0/90]_s$ laminate subjected to a uniform axial strain with few previously published results. Even though, Fig. 2.6(a) shows that the present model predicts a slightly higher interlaminar normal stress at the edges compared to previous studies, the behavior is identical. The shear stress (σ_{23}) distribution is comparable to other models (Fig. 2.6(b)).

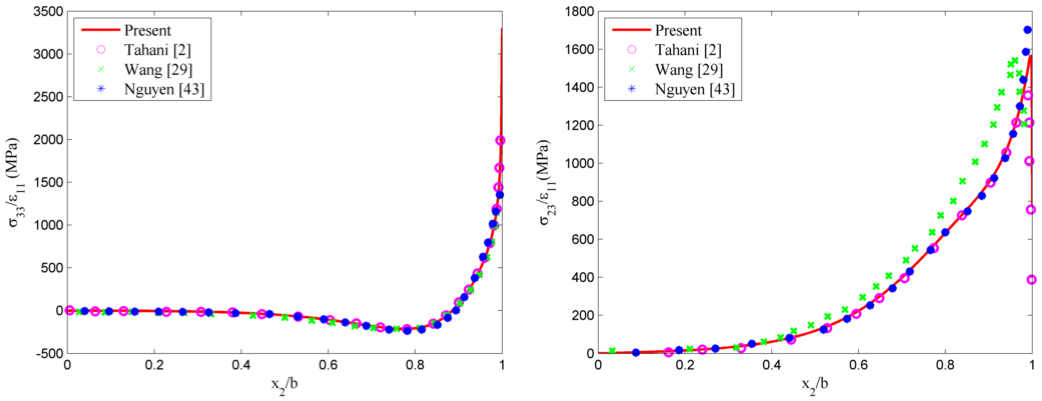

(a) (b)

Figure 2.6: Distribution of interlaminar stresses along the 0/90 interface of [0/90]s laminate subjected to uniform axial extension (a) normal stress σ_{33} and (b) shear stress σ_{23}

For $[45/-45/90/0]_s$ laminate, seldom results were found in the literature to compare the results from the current Q-2D model. In this case, a full 3D model was analyzed and the results from the Q-2D model was compared with the corresponding 3D model. Fig. 2.7 shows the comparison of Q-2D and 3D model at different interfaces, which shows an excellent agreement between these two models.

2.4.2 Case 2: Thermal Loading

In this section, $[0/90]_s$ and $[45/-45/90/0]_s$ laminates subjected to an uniform temperature change ΔT throughout the modeling domain is considered. For direct comparison with the previously published results, the following material properties were used: $E_{11} = 137.9$ GPa, $E_{22} = E_{33} = 14.48$ GPa, $G_{12} = G_{13} = G_{23} = 5.86$ GPa, $\nu_{12} = \nu_{13} = \nu_{23} = 0.21$, $\alpha_1 = 0.36 \times 10^{-6}\ ^\circ C^{-1}$ and $\alpha_2 = \alpha_3 = 28.8 \times 10^{-6}\ ^\circ C^{-1}$. Fig. 2.8 shows the distribution of σ_{33} (Fig. 2.8(a)) and σ_{23} (Fig. 2.8(b)) for $\Delta T = 1\ ^\circ C$. It is observed from Fig. 2.8 that the current results are in excellent agreement with those determined by previous investigators [9, 30, 49].

Fig. 2.9 shows the distribution of interlaminar stresses for $[45/-45/90/0]_s$ laminate along 45/-45 (Fig. 2.9(a)), -45/90 (Fig. 2.9(b)) and 90/0 interfaces (Fig. 2.9(c)) subjected to an uniform temperature change $\Delta T = 1\ ^\circ C$. It is observed from Fig. 2.9 that the current results are in good agreement with the corresponding 3D model results.

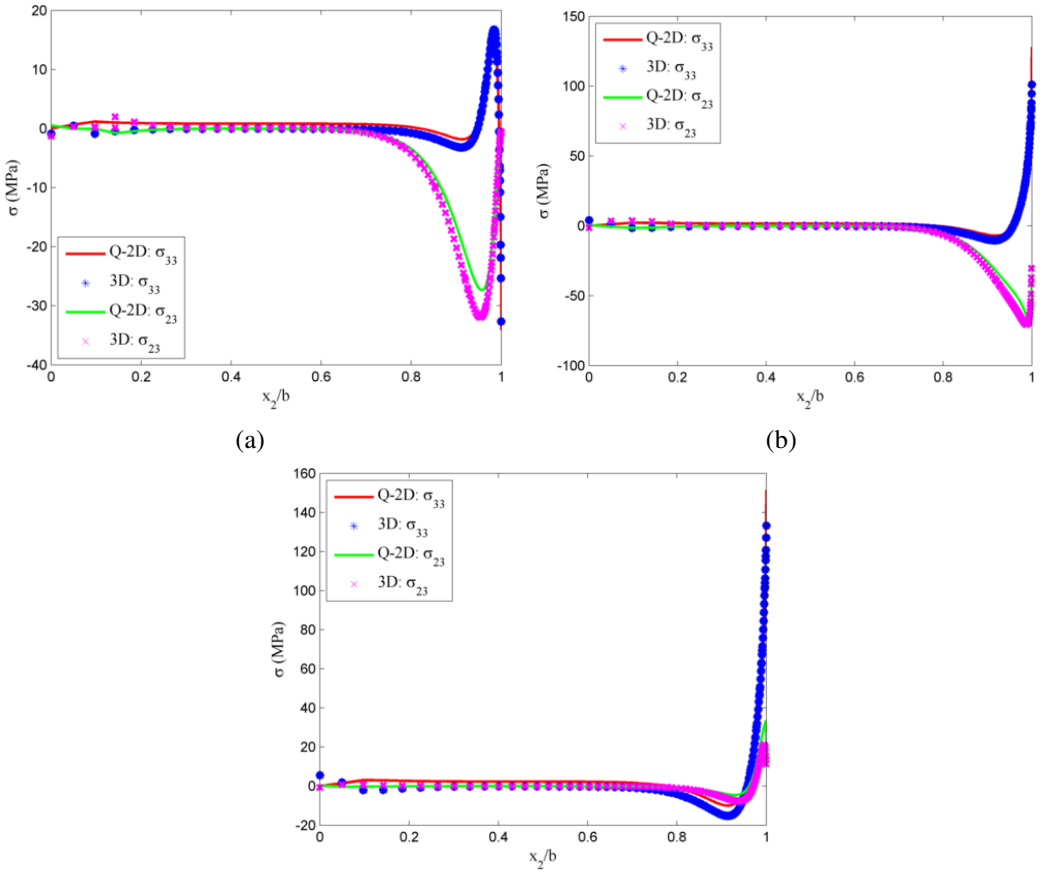

Figure 2.7: Distribution of interlaminar stress of $[45/-45/90/0]_s$ laminate subjected to uniform axial extension along (a) 45/-45, (b) -45/90 and (c) 90/0 interface

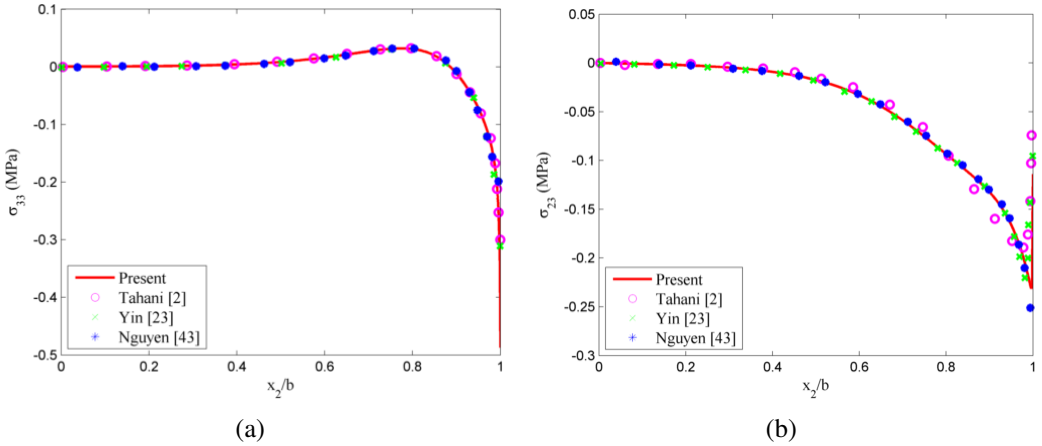

Figure 2.8: Distribution of interlaminar stresses along the 0/90 interface of [0/90]s laminate due to a temperature change $\Delta T = 1\ ^{\circ}C$ (a) normal stress σ_{33} and (b) shear stress σ_{23}

2.4.3 Case 3: Combined Axial and Thermal Loading

In this section, $[0/90]_s$ and $[45/-45/90/0]_s$ laminates subjected to a uniform axial strain ($\epsilon_{11} = 0.01$) and uniform temperature change ($\Delta T = 1^{\circ}C$) is considered. The material properties were

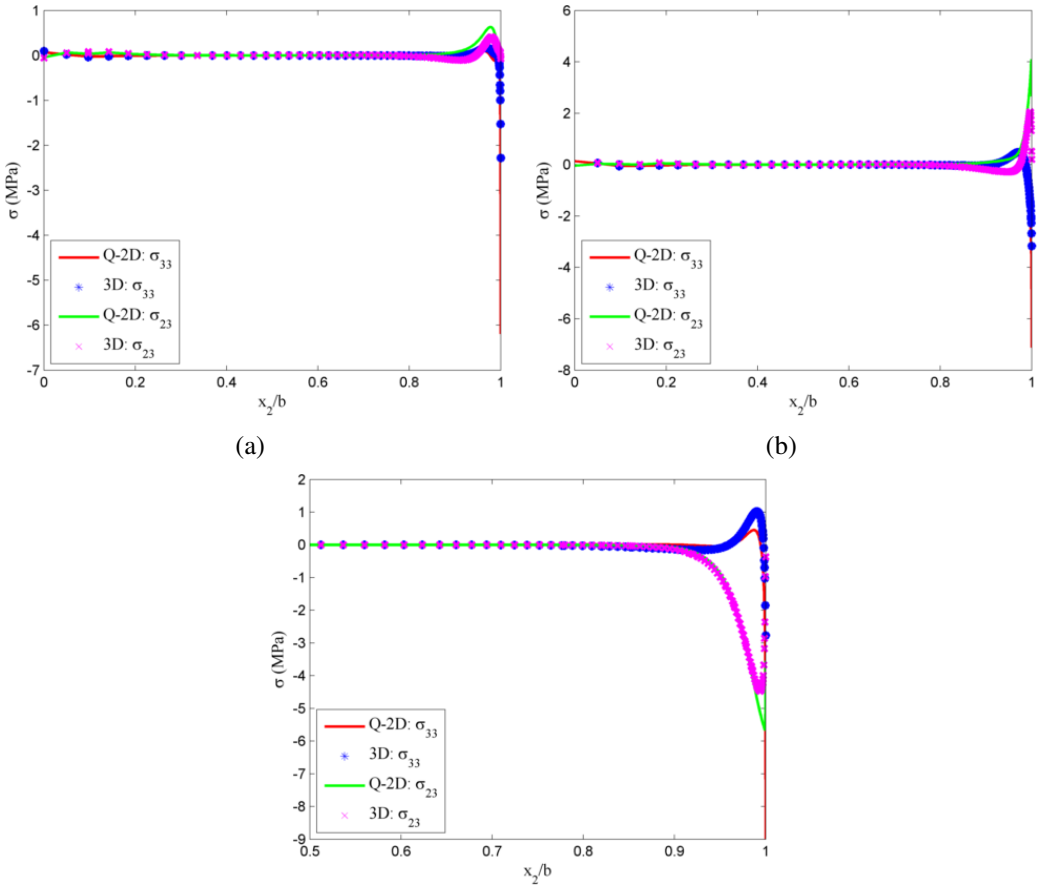

Figure 2.9: Distribution of interlaminar stress of $[45/-45/90/0]_s$ laminate due to a temperature change $\Delta T = 25\ ^\circ C$ (a) 45/-45, (b) -45/90 and (c) 90/0 interface

the same as mentioned in Section 2.4.2. Fig. 2.10 and Fig. 2.11 show the distribution of interlaminar stresses for $[0/90]_s$ and $[45/-45/90/0]_s$ laminates subjected to $\epsilon_{11} = 0.01$ and $\Delta T = 25\ ^\circ C$. These results are compared with their corresponding 3D model and is observed (Fig. 2.10 and Fig. 2.11) that the current results are in excellent agreement with the 3D results.

2.4.4 Efficiency of Q-2D Model

The Q-2D modeling framework developed in this paper utilizes a fairly straight forward derivation and an easy implement within finite element method. It is also highly efficient in computational cost compared to the 3D counterpart models. Table 2.1 shows a comparison of the computational time required by the Q-2D and 3D models of $[45/-45/90/0]_s$ laminate ($\approx$ same time for all loading cases). The total computational time required by Q-2D model is approximately 2 minutes and for the 3D model is approximately 60 minutes using the same Intel® Core™ i7-3540M 3.00 GHz CPU. Although, 60 minutes seems like a reasonable time for a 3D model, it is for only 8 layers laminate ($[45/-45/90/0]_s$). The time required will scale up with increased number of

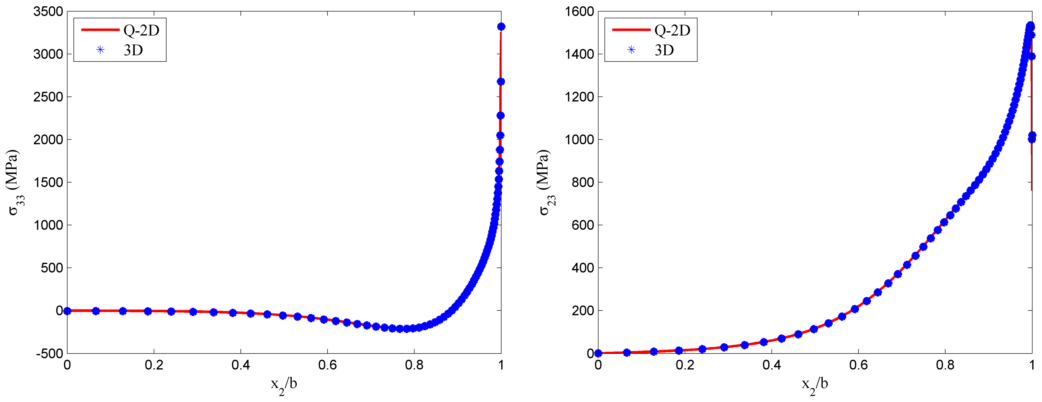

(a) (b)

Figure 2.10: Distribution of interlaminar stress along the 0/90 interface of $[0/90]_s$ laminate subjected to $\epsilon_{11} = 0.01$ and $\Delta T = 25\ ^\circ C$ (a) normal stress σ_{33} and (b) shear stress σ_{23}

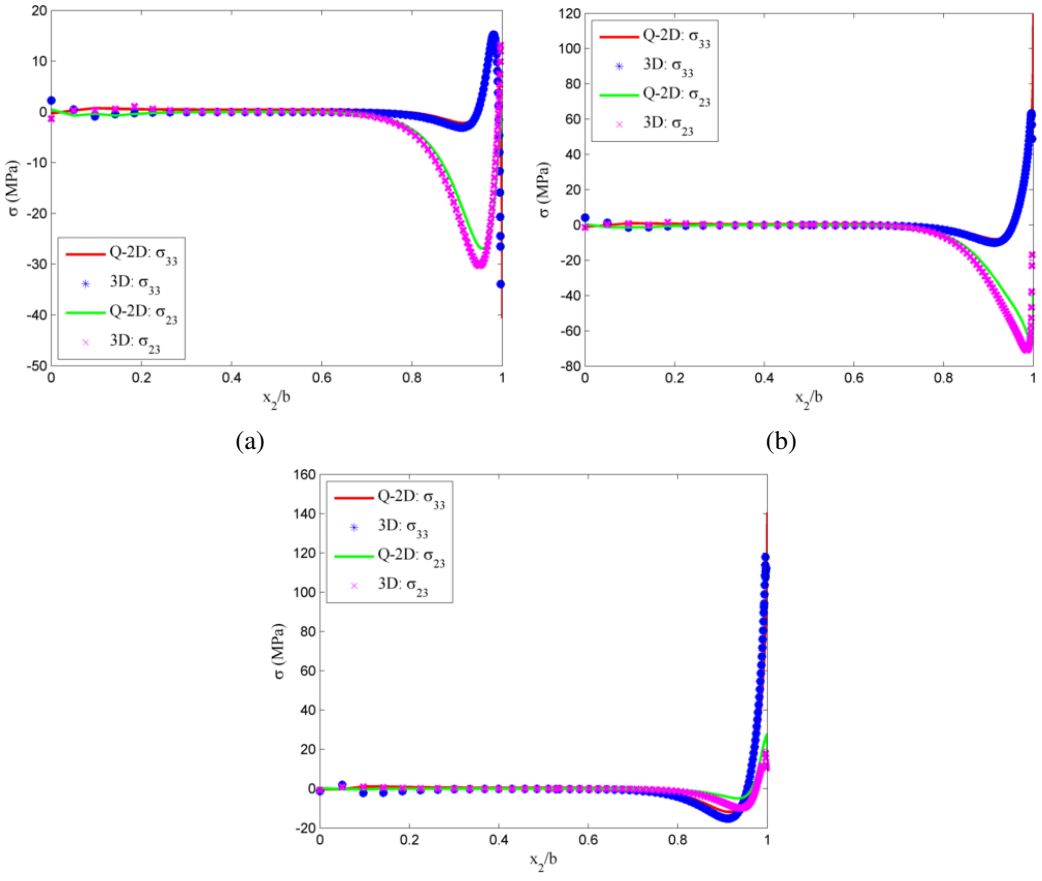

(a) (b)

(c)

Figure 2.11: Distribution of interlaminar stress of $[45/-45/90/0]_s$ laminate subjected to $\epsilon_{11} = 0.01$ and $\Delta T = 25\ ^\circ C$ along (a) 45/-45, (b) -45/90 and (c) 90/0 interface

layers in the case of a thicker laminate (for example 48 layers). Hence, the Q-2D model can save

the computational time significantly while accurately predicting the interlaminar stress distribution.

Table 2.1: Comparison of Q-2D and 3D model

Model	**No. of Elements**	**Approximate Time (min)**
Q-2D	23424	2
3D	318786	60

2.5 Conclusions

In this study, free edge laminates subjected to uniform axial extension and uniform temperature change are investigated with Quasi-2D model. This generalized plane strain model is capable of predicting the interface stresses accurately compared to 3D model. The accuracy and effectiveness of the present Q-2D model is validated with the previously published results and 3D model. This Q-2D model is found to be capable of predicting the interlaminar stresses for different laminates subjected to uniform axial loading and/or thermal loading in a reliable and efficient way.

Chapter 3

Additive Manufacturing for Bonded Composite Joints

3.1 Introduction

Automotive and aerospace industries, amongst many others, are exploring routes to improve the quality of joints in an assembled component. Joints are critical regions in structures due to the stress concentrations manifested compared to the members of a component. With increasing applications of fiber reinforced polymer matrix composites (FRPCs) in aircrafts, navy structures and automobiles, novel joining technology to assist the fabrication of large components has become a priority for structural engineers. Conventional materials such as steel or aluminum are joined using fasteners and/or bolted joints, which is not favorable for FRPCs as drilling or cutting of the composite may damage fibers causing an adverse effect on their structural integrity. Thus, adhesively bonded joints are becoming a viable option for joining FRPCs.

Advantages of bonded joints over traditional mechanical fasteners are lower structural weight and improved damage tolerance. Despite these advantages, bonded joints in primary load-bearing applications often result in overdesign due to the inclusion of mechanical fasteners for additional safety. This is due to the lack of confidence in adhesively bonded joints for composite joining technology. Mechanics based designs for bonded joints are necessary to facilitate efficient use of composites for lightweight applications. This paper presents the use of additive manufacturing to improve the mechanical behavior of bonded joints by enhancing the load bearing capacity of the bond area.

Aerospace industry was the first to conduct work on adhesively bonded joints in the 1970-80s. An extensive review on the joint strength of adhesive joints for fiber reinforced composites was provided by Matthews et al. [52]. New analytical approaches and finite element methods were developed for analyzing bonded joints. The bond strength for FRPCs depends on various parameters, like, joint configuration, adhesive properties, surface preparation, test methods, environmental conditions, etc. Of these, surface preparation is perhaps the most critical in governing the quality of the joint [53]. According to Davis and Bond [54], surface treatment with favorable surface chemistry prior to bonding can result in significant increase in the bond strength resulting in im-

proved durability of adhesive bonds. In order to ensure maximum bond strength, abrasion/solvent cleaning techniques are commonly employed as surface treatment for thermoset composites, like carbon/epoxy or glass/epoxy composites. Other viable options for surface treatments are, grit blasting, acid etching, laser treatment, etc. A novel method is proposed here that utilizes additive manufacturing to impart engineered structure to adherent surfaces in order to drastically increase the bond strength. It is hypothesized that mechanics dictated gradation of interface modification will further assist in improving the strength and toughness of the adhesive bond.

Bonded joints can have different geometries depending on the type of application. Commonly studied joints by previous researchers are single-lap, double-lap, scarf, stepped, T-shaped, tubular lap, L-shaped joints, etc. A detailed procedure for the design of adhesively bonded joints, like single, double and step, for composites under static and cyclic loads is given in Chamis and Murthy [55]. Stress distribution within a joint dictates the strength of an adhesively bonded joint, which in turn depends on the geometry of the joint and material properties of adhesive and adherent. Therefore, a detailed analysis of a joint configuration with the corresponding materials is required to evaluate the stress distribution. The joint design should be catered towards minimizing stress concentrations that catalyze debonding type failure at the composite joint. Especially, peel and cleavage stresses should be suppressed, while maintaining an almost uniform stress distribution along the joint. The effects of stress concentrations are accentuated due to layered nature of fiber reinforced composites. The weak interfaces within the adherents can result in their failure along with joint failure. Therefore, it is essential to improve the mechanical properties of bonded joint regions of a layered composite.

Single-lap joint is one of the most commonly used joint geometry due its simplicity and easiness to fabricate. However, stress concentrations are manifested at the ends of the bond overlap that potentially cause damage resulting in the premature failure of a bonded joint. Earlier researchers have explored modifying the adherent geometries ([56] [57] [58]), like tapering, stepping and wavy lap, as possible options to minimize these stress concentrations to improve their load bearing capacity. However, a changing adherent shape is a constraint on the component geometry and may not be favorable for fabrication purposes. Hence, there is a critical need to improve the bond strength while maintaining standard geometries of the adherent. Further, complex joint designs, like T-joint or Pi-joint, that are used to join composites require extensive investigation on the stress distribution and its influence on the overall structural integrity of the component.

Motivation

Interface design is very critical for bonded joints in FRPCs and a smart designing technique should be developed to minimize the damage and failure incurred by weak bond interfaces. It is hypothesized that improvement in strength and toughness can be achieved by imparting structural texture at the adhesively bonded joint interfaces. Hence, novel technology using additive manufacturing at the bond interfaces has been explored in this paper.

The research reported in this paper was split into the following main steps: 1) Conduct single lap shear (SLS) tests on pure epoxy adhesively bonded joints to establish a baseline for apparent shear strength; 2) Analyze the bonded joint systems computationally to determine the stress distributions; 3) Modify the bond design computationally to understand their influence on the distribution of stresses; 4) Enable the optimum designs at the bond regions accurately using fused

deposition modeling within polymer additive manufacturing; 5) Conduct single lap shear (SLS) tests on the new designs to check the influence of the new bond interface designs on the apparent shear strength.

The outline of the paper is as follows: The manufacturing process for pure adhesively bonded joints and additively manufactured joints is explained first, followed by the computational modeling of altered bond designs. The experimental approach for testing the single lap joints is described next followed by results, discussion and conclusions.

3.2 Manufacturing

Single lap shear adhesively bonded joints were examined in this paper following the ASTM D5868-01 standard. The manufacturing process of the bonded joints can be divided into two parts: (1) development of bonded joints using pure adhesive only, and (2) development of the bonded joints incorporating 3D printed designs on the adherents. The joint preparation process for both cases will be discussed next.

3.2.1 Pure Adhesive Joints

Two carbon fiber laminate adherents were bonded together with LOCTITE Hysol E-120HP epoxy that was cured at room temperature for 24 hours. The adherent substrates used were water-jet cut from a DragonPlate solid carbon fiber laminate (3/31" Matte 12"x 24"). A total of 5 joints with dimension shown in Fig. 3.1 were fabricated and tested.

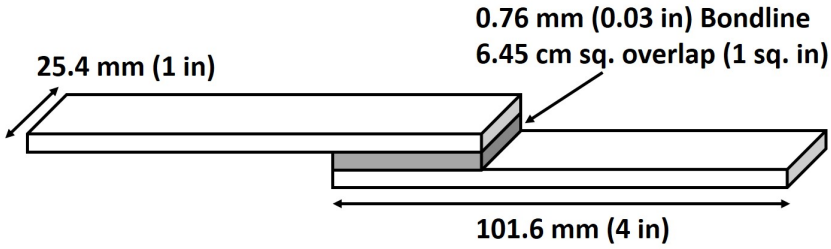

Figure 3.1: Dimensions for single lap joint as per the ASTM standard.

Bond line thickness of 0.76 mm was achieved using glass microspheres, which provided a bond line control of 700-800 microns. A mass ratio of 10:1 between adhesive and microspheres was implemented. The microspheres were mixed thoroughly with the resin prior applying on to the substrates over an overlap area of 6.45 cm^2. Pressure was exerted on the overlap area using c-clamps (see Fig. 3.2). In order maintain the same applied pressure on each joint fabricated, it was ensured to maintain the equal number of threads above the c-clamp overhead for each, thus, regulating equal pressures for all samples.

Figure 3.2: C-clamps were used for applying constant pressure.

3.2.2 3D-Printed Adhesive Joints

Manufacturing 3D-printed adhesive (3D-PA) joints using fused deposition modeling (FDM) required printing the designs on to the carbon fiber adherents (or substrates) prior to fabricating the joints using epoxy. FORTUS 900mc Stratasys machine was the printer used located within the W. M. Keck Center for 3D Innovation at the University of Texas at El Paso. The material used to create interface designs was ABS-M30, which will be referred to as "model" material in this paper. ABS-M30 is up to 25-70 percent stronger than standard Stratasys ABS material, possessing greater tensile, impact, and flexural strength. The model material was extruded at a temperature of 315 C, the support extrusion temperature was 320 C, and the chamber temperature was 95 C. Note that these temperatures vary for different model materials, such as polycarbonate (PC) or ULTEM 9085. Prior to starting printing the model material onto the substrates (or adherents), they were exposed to the chamber temperature for ABS-M30 for fifteen minutes to check for any damage imparted due to the chamber temperature. The substrates showed no degradation in the material property and the printing process was initiated next.

Due to the lack of a standard manufacturing procedure for 3D printing over carbon-fiber substrates, a new methodology was developed and followed for printing above the nominal thickness of the substrates. 3D printing machines are generally calibrated in the x, y, and z directions for printing over their corresponding platforms, but, lack the same for composite substrates.

An overview of the fabrication procedure is described here. First, a design resembling teeth-shaped lines was developed using CAD software. The slice height parameter was set to 0.007 in, which derived in a four layer stack up for the desired 0.03 in bond control thickness. Because of this, no microspheres were mixed with the resin since the bond line control was achieved by the printed design itself. These lines are intended for reinforcing the through-thickness interface of the joint, resisting shear from any mode II stimuli applied - this will be discussed later. After this, an enclosure box with the nominal thickness (z direction) of the substrates was added below the teeth-shaped lines to ensure two things: (1) that lines printed exactly over the enclosed box where the substrate will be placed and (2) that it constraints the movement of the composite in the three directions. This box, at first, was filled with support material, but was removed later using Stratasys Insight software (see Fig. 3.3). A pause was inserted in the beginning layer of the teeth lines - this way, once the box was built with no support, the printer would automatically stop, allowing the user to place the substrate inside the box, and resume the printing job at hand. Printing time of the

final .stl file used was approximately ten minutes.

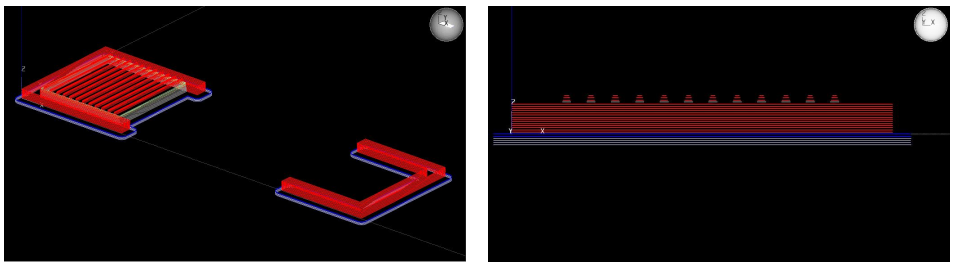

Figure 3.3: (a) Isometric view of enclosure box with teeth lines; (b) Side view zoom of area of interest.

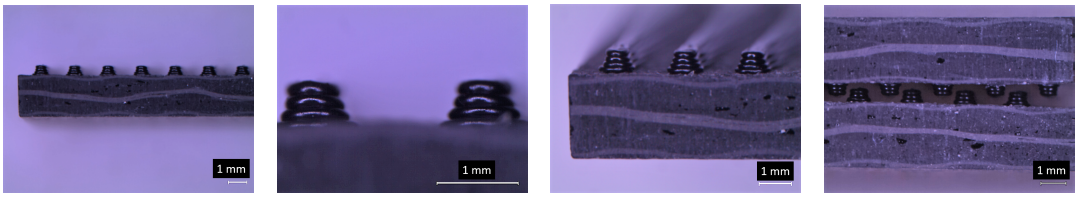

Figure 3.4: (a) Isometrc view of 3D printed output; (b) Visible gaps in side view of lap joint.

Fig. 3.4 shows the side view of the printed specimens. The spacing between the design lines were adjusted such that there is enough space for a resin layer between them to assist perfect bonding in the lap joint. Overall, the 3D printing process involved the following steps:

- Prepare CAD file of the design and enclosure box using SolidWorks.
- Pre-processing of CAD: deleting support and adding a pause layer using Insight software.
- Build the output file in the FORTUS 900mc machine, and insert the substrate when the pause layer begins. Then, resume build.
- If bond strength between ABS-M30 and carbon fiber is as desired, proceed to build next file. If not, calibrate machine in the z direction and re-build until desired bond strength is reached.

Upon printing the designs on the substrates, the procedure for fabricating the single lap joints was identical to the pure adhesive joints case, except microspheres were not used here as the designs provided the required bond size.

3.3 Computational Approach

A computational model of the bonded joint specimen was developed (see Fig. 3.5) to determine the stress distribution in the bond regions. Commercially available finite element method software

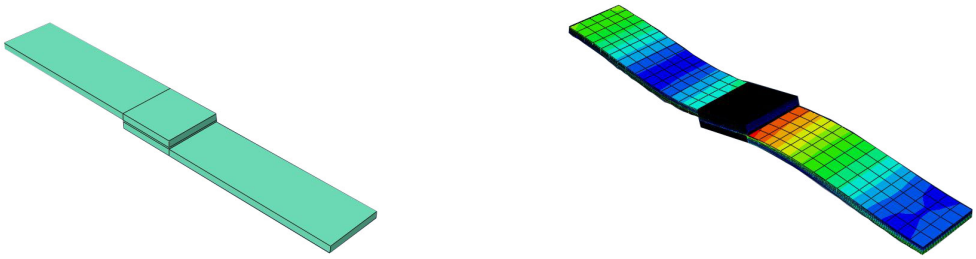

Figure 3.5: (a) Undeformed finite element model; (b) Deformed finite element model.

"ABAQUS" was used to model the system. Due to the complexity of the structure within carbon fiber laminates, a simplified homogenized model for the adherents was developed.

The effective mechanical properties of the carbon fiber laminate (adherents), adhesive and the model material (3D printed) are shown in Table 3.1.

Material	Young's Modulus (PSI)	Poisson's Ratio
Adherents	30,000,000	0.3
Adhesive	1,500,000	0.3
Reinforcement ABS-30M	400,000	0.3

Table 3.1: List of materials and their assumed mechanical properties

The first model generated was the bonded joint specimen with pure epoxy. The loading condition applied was a 0.04" displacement in tension at both ends of the specimen along the x-direction. Maximum principal stress and strain were plotted along the centerline of the bonded region as shown in Fig. 3.6.

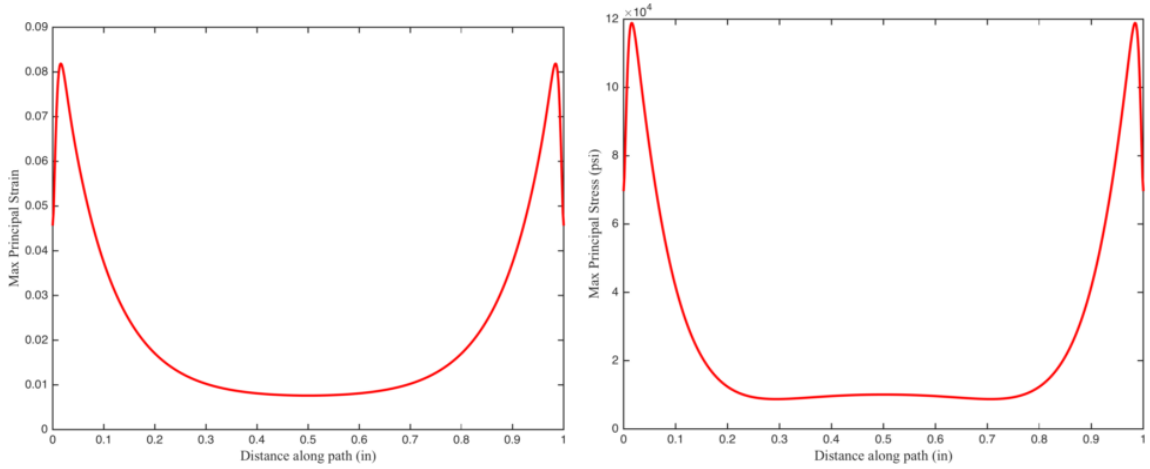

Figure 3.6: (a) Maximum principal strain along center path; (b) Maximum principal stress along bonded region center path

This was followed by modeling the bond region with different designs as shown in Fig. 3.7. Four distinct models with different spacing between the 3D printed lines were developed and simu-

lated. In the pure epoxy model, the bonded regions experienced significant stress and strain towards the edges of the bonded region [59]. Due to these significant stresses and strains, the material is more likely to initiate failure in these regions. The prime objective of the designs imparted to the bonded interface is to evenly redistribute the stresses and strains to effectively reduce the risk of failure, thus improving the strength of the adhesively bonded joints.

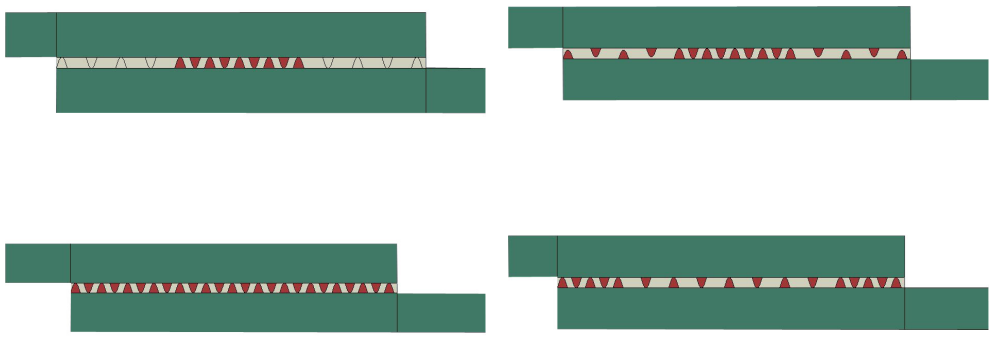

Figure 3.7: (a) Model 1; (b) Model 2; (c) Model 3; (d) Model 4.

The stress distribution was determined for each case, and the results are shown in Fig. 3.8.

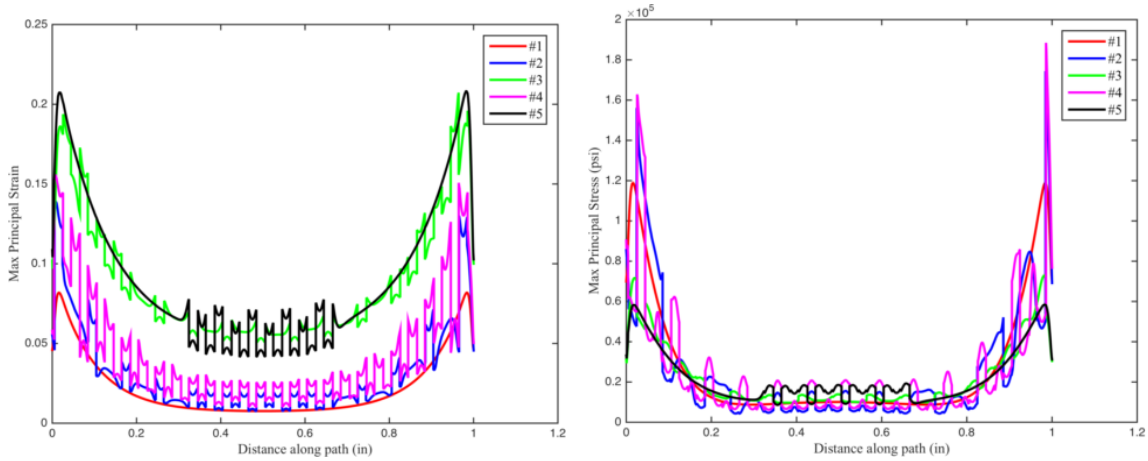

Figure 3.8: (a) Principal strain for pure epoxy and 4 models; (b) Principal stress for pure epoxy and 4 models.

It is hypothesized that the models with uniform stress distribution and lower edge stresses compared to the pure adhesive case are expected to display higher resistance to bond failure. This will be validated through SLS tests of the printed samples, where it is expected that higher shear strengths will be observed for those models.

3.4 Experimental Approach

Single lap shear tests were conducted to determine the apparent shear strength of the single lap joint bonded specimens. Pure epoxy adhesive and 3D-PA joints were tested in the same manner.

3.4.1 Mode-II Tensile Testing of the Lap Shear Joints

Tensile tests were performed on an INSTRON 5696 machine, assuring safety conditions and following protocol regulations [60] and specifications mentioned in ASTM D5868-014 [61]. The initial grip separation was 75 mm with 25.4 mm minimum grip length for samples at each end. The specimen loading rate was 13 mm/min. Five samples for each bond type were prepared as mentioned before and tested. Fig. 3.9 shows the experimental set up for the lap shear test.

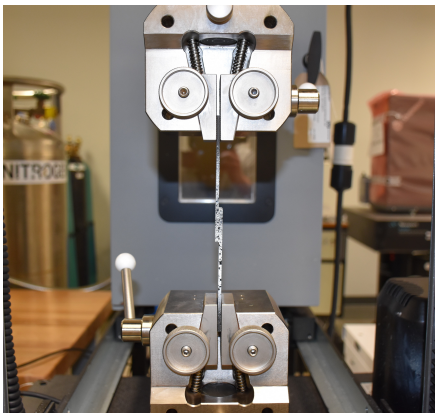

Figure 3.9: Experimental set up of shear lap tests

3.5 Results and Discussion

The SLS data obtained from the INSTRON machine was post-processed to determine the apparent shear strength of the bonded joints. According to the ASTM standard, individual peak load values (KPa), failure type, and averages by maximum and minimum values were determined. Failure type of the lap joints was decided based on the criteria shown in Fig. 3.10.

The results for the pure epoxy bonded joints are discussed first followed by the 3D-PA bonded joints. A discussion of the comparison of the outputs from all cases will be conducted in a later section.

3.5.1 Pure Adhesive Bonded Joints

The peak loads determined from the SLS tests for PA bonded joints are given in Table 3.2. The shear stress in each case was calculated by dividing the peak load by the bond area.

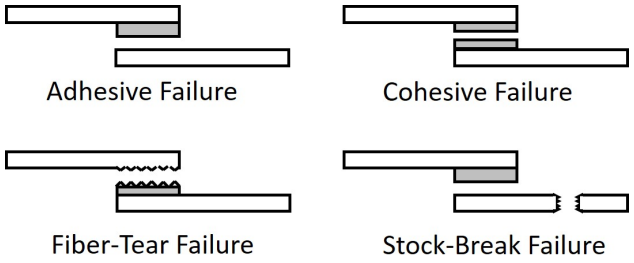

Figure 3.10: Failure types in lap shear tests.

Joint	Peak Load (N)	Shear Stress (MPa)	Failure Type
1	680.38	35.15	Adhesive
2	1256.08	64.90	Adhesive
3	808.92	41.79	Adhesive
4	13546	699.88	Cohesive
5	1130.91	58.43	Adhesive

Table 3.2: Post-processing results for pure epoxy joints.

Adhesive and cohesive failure were the two key failure modes observed from the five joints tested. Adhesive failures can be observed in Fig. 3.11(a), where the bond region separates from the adherent completely. Note that the glass microspheres are visible in this figure. Cohesive failure was observed in one case only as shown in Fig. 3.11(b), where the failure region passed through the bond material. Cohesive failure was ignored due to its rare occurrence within the 5 pure epoxy bonded joints tested.

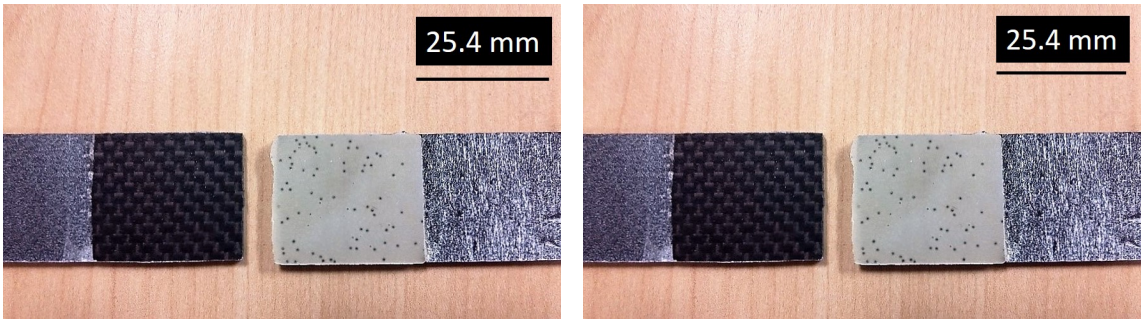

Figure 3.11: (a) Top view of adhesive failure; (b) Top view of cohesive failure.

3.5.2 3D-Printed Adhesive Bonded Joints

The SLS test results for the four 3D-PA bonded joints will be discussed individually. The data format is the same as in the case of PA adhesive joints, as per the standard.

3D-PA Joints: Model 1

Table 3.3 represents the peak load, shear strength and failure types for 3D-PA Model-1 adhesive

joints.

Joint	Peak Load (N)	Shear Stress (MPa)	Failure Type
1	4102.82	212.53	Adhesive
2	5254.18	272.18	Cohesive
3	3755.47	194.54	Adhesive
4	3943.09	204.26	Adhesive
5	4610.36	238.83	Adhesive

Table 3.3: Post-processing results for model 1 joints.

Model-1 3D-PA bonded joints displayed adhesive and cohesive failures at the bond region as shown in Fig. 3.12. Note that the 3D designs are visible in both types of failure. It should be noted that the corresponding peak loads and stresses increased significantly compared to the PA joints.

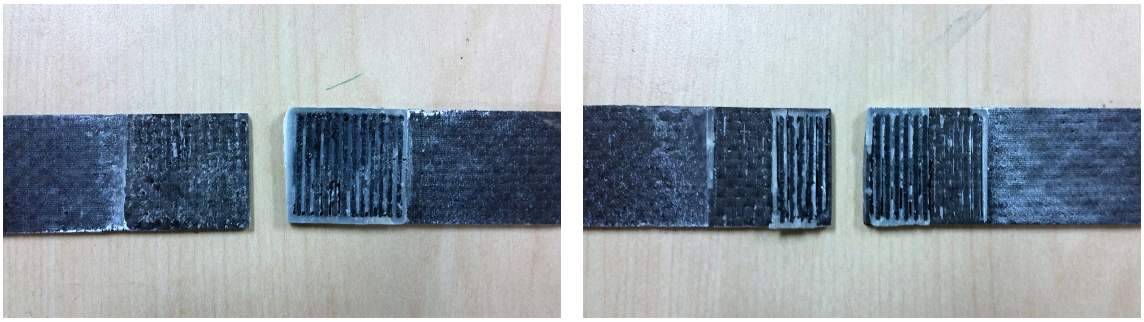

Figure 3.12: (a) Top view of adhesive failure; (b) Top view of cohesive failure.

3D-PA Joints: Model 2

Joint	Peak Load (N)	Shear Stress (MPa)	Failure Type
1	6551.08	338.47	Cohesive
2	4778.79	246.9	Adhesive
3	6851.07	353.97	Cohesive
4	7755.10	400.68	Cohesive

Table 3.4: Post-processing results for model 2 joints.

3.5.3 Conclusion: Pure Adhesive vs. 3D-Printed Adhesive Bonded Joints

This initial study has shown that the structure imparted to the bond regions using 3D printing has significantly improved the shear strength of the bonded joints. Current ongoing work focuses on printing the remaining designs that were computationally analyzed to test the hypothesis stated before. Further study will investigate the influence of optimized design on the strength of pi-joints.

Bibliography

[1] S. H. Lee and A. M. Waas. Compressive response and failure of fiber reinforced unidirectional composites. *International Journal of Fracture*, 100:275–306, 1999.

[2] S. H. Lee, C. S. Yerramalli, and A. M. Waas. Compressive splitting response of glass-fiber reinforced unidirectional composites. *Composites Science and Technology*, 60:2957–2966, 2000.

[3] T. J. Vogler, S. Y. Hsu, and S. Kyriakides. On the initiation and growth of kink bands in fiber composites. part ii: analysis. *International Journal of Solids and Structures*, 38:2653–2682, 2001.

[4] S. Pimenta, R. Gutkin, S. T. Pinho, and P. Robinson. A micromechanical model for kink-band formation: Part i experimental study and numerical modelling. *Composites Science and Technology*, 69:948–955, 2009.

[5] S. Pimenta, R. Gutkin, S. T. Pinho, and P. Robinson. A micromechanical model for kink-band formation: Part ii analytical modelling. *Composites Science and Technology*, 69:956–964, 2009.

[6] C. S. Yerramalli and A. M. Waas. A failure criterion for fiber reinforced polymer composites under combined compression-torsion loading. *International Journal of Solids and Structures*, 40(5):1139–1164, 2003.

[7] Pavana Prabhakar and Anthony M. Waas. Micromechanical modeling to determine the compressive strength and failure mode interaction of multidirectional laminates. *Composites Part A: Applied Science and Manufacturing*, 50:11 – 21, 2013.

[8] D. Zhang, J. Ye, and H.Y. Sheng. Free-edge and ply cracking effect in cross-ply laminated composites under uniform extension and thermal loading. *Composite structures*, 76(4):314–325, 2006.

[9] M. Tahani and A. Nosier. Free edge stress analysis of general cross-ply composite laminates under extension and thermal loading. *Composite Structures*, 60(1):91–103, 2003.

[10] A.H. Puppo and H.A. Evensen. Interlaminar shear in laminated composites under generalized plane stress. *Journal of composite materials*, 4(2):204–220, 1970.

[11] N.J. Pagano. On the calculation of interlaminar normal stress in composite laminate. *Journal of Composite Materials*, 8(1):65–81, 1974.

[12] P.W. Hsu and C.T. Herakovich. Edge effects in angle-ply composite laminates. *Journal of Composite Materials*, 11(4):422–428, 1977.

[13] S. Tang. A boundary layer theory-part i: Laminated composites in plane stress. *Journal of composite materials*, 9(1):33–41, 1975.

[14] J.L. Davet and Ph. Destuynder. Free-edge stress concentration in composite laminates: A boundary layer approach. *Computer methods in applied mechanics and engineering*, 59(2):129–140, 1986.

[15] C.C. Lin and C.C. Ko. Method for calculating the interlaminar stresses in symmetric laminates containing a circular hole. *AIAA journal*, 30(1):197–204, 1992.

[16] R.B. Pipes and N.J. Pagano. Interlaminar stresses in composite laminatesan approximate elasticity solution. *Journal of Applied Mechanics*, 41(3):668–672, 1974.

[17] N.J. Pagano. Stress fields in composite laminates. *International Journal of Solids and Structures*, 14(5):385–400, 1978.

[18] S.G. Leknitskii and P. Fern. *Theory of elasticity of an anisotropic elastic body*. Holden-Day, 1963.

[19] S.S. Wang and I. Choi. Boundary-layer effects in composite laminates: Part 1free-edge stress singularities. *Journal of Applied Mechanics*, 49(3):541–548, 1982.

[20] S.S. Wang and I. Choi. Boundary-layer effects in composite laminates: Part 2free-edge stress solutions and basic characteristics. *Journal of Applied Mechanics*, 49(3):549–560, 1982.

[21] S.S. Wang and I. Choi. The interface crack between dissimilar anisotropic composite materials. *Journal of applied mechanics*, 50(1):169–178, 1983.

[22] S.S. Wang and I. Choi. The interface crack behavior in dissimilar anisotropic composites under mixed-mode loading. *Journal of applied mechanics*, 50(1):179–183, 1983.

[23] C. Kassapoglou and P.A. Lagace. An efficient method for the calculation of interlaminar stresses in composite materials. *Journal of Applied Mechanics*, 53(4):744–750, 1986.

[24] C. Kassapoglou and P.A. Lagace. Closed form solutions for the interlaminar stress field in angle-ply and cross-ply laminates. *Journal of Composite Materials*, 21(4):292–308, 1987.

[25] J.P.H. Webber and S.K. Morton. An analytical solution for the thermal stresses at the free edges of laminated plates. *Composites science and technology*, 46(2):175–185, 1993.

[26] W. Becker. Closed-form solution for the free-edge effect in cross-ply laminates. *Composite Structures*, 26(1):39–45, 1993.

[27] C. Kassapoglou. Determination of interlaminar stresses in composite laminates under combined loads. *Journal of reinforced plastics and composites*, 9(1):33–58, 1990.

[28] W.L. Yin. Free-edge effects in anisotropic laminates under extension, bending and twisting, part i: a stress-function-based variational approach. *Journal of Applied Mechanics*, 61(2):410–415, 1994.

[29] W.L. Yin. Free-edge effects in anisotropic laminates under extension, bending, and twisting, part ii: eigenfunction analysis and the results for symmetric laminates. *Journal of Applied Mechanics*, 61(2):416–421, 1994.

[30] W.L. Yin. The effect of temperature gradient on the free-edge interlaminar stresses in multilayered structures. *Journal of composite materials*, 31(24):2460–2477, 1997.

[31] R.B. Pipes and N.J. Pagano. Interlaminar stresses in composite laminates under uniform axial extension. *Journal of Composite Materials*, 4(4):538–548, 1970.

[32] E. Altus, A. Rotem, and M. Shmueli. Free edge effect in angle ply laminates- a new three dimensional finite difference solution. *Journal of Composite Materials*, 14:21–30, 1980.

[33] K. Bhaskar, T.K. Varadan, and C. Jacob. Free edge stresses in laminated cylindrical shells due to axisymmetric transverse loads. *JOURNAL-AERONAUTICAL SOCIETY OF INDIA*, 52(1):26–38, 2000.

[34] N.J. Salamon. Interlaminar stressess in a layered composite laminate in bending. *Fibre Science and Technology*, 11(4):305–317, 1978.

[35] A.S.D. Wang and F.W. Crossman. Some new results on edge effect in symmetric composite laminates. *Journal of Composite Materials*, 11(1):92–106, 1977.

[36] A.S.D. Wang and F.W. Crossman. Edge effects on thermally induced stresses in composite laminates. *Journal of Composite Materials*, 11(3):300–312, 1977.

[37] C.T. Herakovich, G.D. Renieri, and H.F. Brinson. Finite element analysis of mechanical and thermal edge effects in composite laminates. In *Army Symposium on Solid Mechanics, Composite Materials: The Influence of Mechanics of Failure on Design, Cape Cod (USA)*, pages 237–248, 1976.

[38] G. Isakson and A. Levy. Finite-element analysis of interlaminar shear in fibrous composites. *Journal of Composite Materials*, 5(2):273–276, 1971.

[39] E.F. Rybicki. Approximate three-dimensional solutions for symmetric laminates under inplane loading. *Journal of Composite Materials*, 5(3):354–360, 1971.

[40] J.Y. Kim and C.S. Hong. Three-dimensional finite element analysis of interlaminar stresses in thick composite laminates. *Computers & structures*, 40(6):1395–1404, 1991.

[41] U. Icardi and A.M. Bertetto. An evaluation of the influence of geometry and of material properties at free edges and at corners of composite laminates. *Computers & structures*, 57(4):555–571, 1995.

[42] L.B. Lessard, A.S. Schmidt, and M.M. Shokrieh. Three-dimensional stress analysis of free-edge effects in a simple composite cross-ply laminate. *International Journal of Solids and Structures*, 33(15):2243–2259, 1996.

[43] S. Yi and H.H. Hilton. Finite element analysis of free edge stresses in non-linear viscoelastic composites under uniaxial extension, bending and twisting loadings. *International journal for numerical methods in engineering*, 40(22):4225–4238, 1997.

[44] R.L. Spilker and S.C. Chou. Edge effects in symmetric composite laminates- importance of satisfying the traction-free-edge condition. *Journal of Composite Materials*, 14:2–20, 1980.

[45] C.Y. Lee and J.M. Chen. Interlaminar shear stress analysis of composite laminate with layer reduction technique. *International journal for numerical methods in engineering*, 39(5):847–865, 1996.

[46] D.H. Robbins and J.N. Reddy. Variable kinematic modelling of laminated composite plates. *International Journal for Numerical Methods in Engineering*, 39(13):2283–2317, 1996.

[47] P. Gaudenzi, A. Mannini, and R. Carbonaro. Multi-layer higher-order finite elements for the analysis of free-edge stresses in composite laminates. *International journal for numerical methods in engineering*, 41(5):851–873, 1998.

[48] E. Martin, D. Leguillon, and N. Carrère. A twofold strength and toughness criterion for the onset of free-edge shear delamination in angle-ply laminates. *International journal of Solids and Structures*, 47(9):1297–1305, 2010.

[49] V.T. Nguyen and J.F. Caron. Finite element analysis of free-edge stresses in composite laminates under mechanical an thermal loading. *Composites Science and Technology*, 69(1):40–49, 2009.

[50] R.P. Carreira, J.F. Caron, and A.D. Diaz. Model of multilayered materials for interface stresses estimation and validation by finite element calculations. *Mechanics of materials*, 34(4):217–230, 2002.

[51] S.H. Lo, W. Zhen, Y.K. Cheung, and C. Wanji. An enhanced global–local higher-order theory for the free edge effect in laminates. *Composite structures*, 81(4):499–510, 2007.

[52] F. L. Matthews, P. P. F. Kilty, and E. Godwin. A review of the strength of joints in fiber-reinforced plastics 2: adhesively bonded joints. *Composites*, 13(1):2937, 1982.

[53] A. Baldan. Adhesively-bonded joints and repairs in metallic alloys, polymers and composite materials: adhesives, adhesion theories and surface pretreatment. *J.Mater. Sci.*, 39(1):1 – 49, 2004.

[54] M. J. Davis and D. Bond. Principles and practise of adhesive bonded structural joints and repairs. *Int. J. Adhesion Adhes.*, 19(3):91 – 105, 1999.

[55] C. C. Chamis and P. L. N. Murthy. Simplified procedures for designing adhesively bonded composite joints. *J. Reinf. Plast. Compos.*, 10(1):29 – 41, 1991.

[56] J.-S. Kim, C. G. Kim, and C. S. Hong. Practical design of tapered composite structures using the manufacturing cost concept. *Compos. Struct.*, 51(3):285299, 2001.

[57] R. H. Kaye and M. Heller. Through-thickness shape optimisation of bonded repairs and lap-joints. *Int. J. Adhesion Adhes.*, 22(1):7 – 21, 2002.

[58] L. F. M. da Silva and R. Adams. Techniques to reduce the peel stresses in adhesive joints with composites. *Int. J. Adhesion Adhes.*, 27(3):227235, 2007.

[59] T.P. Lang and P.K. Mallick. The effect of recessing on the stresses in adhesively bonded single-lap joints. *International Journal of Adhesion and Adhesives*, 19(4):257 – 271, 1999.

[60] S. K. Mazumdar and P. K. Mallick. Static and fatigue behavior of adhesive joints in smc-smc composites. *Polymer Composites 19*, 2(1):139–146, 1998.

[61] ASTM(D5868-014). Standard test method for lap shear adhesion for fiber reinforced plastic (frp) bonding. 2014.

AFOSR Deliverables Submission Survey

Response ID:6746 Data

1.

Report Type

Final Report

Primary Contact Email

Contact email if there is a problem with the report.

ehzazueta@utep.edu

Primary Contact Phone Number

Contact phone number if there is a problem with the report

(915) 747-7351

Organization / Institution name

The University of Texas at El Paso

Grant/Contract Title

The full title of the funded effort.

A Novel Multiscale Design of Interfaces for Polymeric Composites and Bonded Joints using Additive Manufacturing

Grant/Contract Number

AFOSR assigned control number. It must begin with "FA9550" or "F49620" or "FA2386".

FA9550-15-1-0216

Principal Investigator Name

The full name of the principal investigator on the grant or contract.

Prabhakar, Pavana

Program Officer

The AFOSR Program Officer currently assigned to the award

Dr. David Stargel

Reporting Period Start Date

05/01/2015

Reporting Period End Date

08/31/2016

Abstract

Interfaces in polymer based carbon fiber composites are critical regions that are most susceptible to delamination under static and impact loads. Debonding or delamination is observed to be a significant failure mechanism in layered composites with significant visible damage. A computational modeling approach is being developed to obtain optimized designs for interfaces and upscale the influence of interface reinforcements for damage and failure resistant designs, which will aid in improving the overall performance of the composite. Polymer additive manufacturing techniques are being explored towards constructing these optimized microscale interface designs based on the suggestions from the computational models.

Distribution Statement

This is block 12 on the SF298 form.

Distribution A - Approved for Public Release

Explanation for Distribution Statement

DISTRIBUTION A: Distribution approved for public release.

If this is not approved for public release, please provide a short explanation. E.g., contains proprietary information.

SF298 Form

Please attach your SF298 form. A blank SF298 can be found here. Please do not password protect or secure the PDF The maximum file size for an SF298 is 50MB.

SF298 Final Report PI Pavana Prabhakar - Award No FA9550-15-1-0216.pdf

Upload the Report Document. File must be a PDF. Please do not password protect or secure the PDF . The maximum file size for the Report Document is 50MB.

Final Report PI Pavana Prabhakar - Award No FA9550-15-1-0216.pdf

Upload a Report Document, if any. The maximum file size for the Report Document is 50MB.

Archival Publications (published) during reporting period:

No

New discoveries, inventions, or patent disclosures:
Do you have any discoveries, inventions, or patent disclosures to report for this period?

No

Please describe and include any notable dates

Do you plan to pursue a claim for personal or organizational intellectual property?

Changes in research objectives (if any):

No

Change in AFOSR Program Officer, if any:

No

Extensions granted or milestones slipped, if any:

No

AFOSR LRIR Number

LRIR Title

Reporting Period

Laboratory Task Manager

Program Officer

Research Objectives

Technical Summary

Funding Summary by Cost Category (by FY, $K)

	Starting FY	FY+1	FY+2
Salary			
Equipment/Facilities			
Supplies			
Total			

Report Document

Report Document - Text Analysis

Report Document - Text Analysis

Appendix Documents

2. Thank You

E-mail user

Aug 29, 2016 18:23:17 Success: Email Sent to: ehzazueta@utep.edu